Carnegie Observatories Astrophysics Series, Vol. 4:
Origin and Evolution of the Elements, 2004
ed. A. McWilliam and M. Rauch (Cambridge: Cambridge Univ. Press)

Metal Ejection by Galactic Winds

CRYSTAL L. MARTIN
University of California, Santa Barbara

Abstract

The development of high-resolution X-ray spectral imaging has made it possible to constrain the metal content of hot galactic winds and to explore the relationship between cold, warm, and hot gas in galactic outflows. I review the empirically derived limits on metal ejection and mass loss rates and discuss their variation with galactic mass. I use these results to normalize standard leaky-box models of chemical evolution and examine the galactic chemical properties that they predict. The amount of intergalactic metal enrichment by starburst winds is also discussed.

1.1 Introduction

In a little over a decade, our knowledge of galactic winds has grown from a theoretical parameter to a phenomenon studied at nearly every electromagnetic frequency. This widespread effort is fueled by the increasing recognition of the large number of high-redshift galaxies with massive outflows (e.g., Pettini et al. 2002; Adelberger et al. 2003), and the relevance of winds for the properties of galaxies and intergalactic gas.

This review concentrates on measurements of the metal content and mass flow rate in winds, with an emphasis on nearby galaxies. I begin with a simplified theoretical description of the coupling between supernovae and the interstellar medium (ISM), which illustrates the multi-phase nature of winds. I then describe the X-ray observations and analysis techniques that constrain the mass and metallicity of the hot wind. I summarize the variation in X-ray properties with the gravitational potential depth and draw attention to the biased view provided by observations of emission processes. I then review the known absorption-line signatures of winds in some detail and speculate about the connections to some classes of intervening absorption-line systems. Finally, I combine the information afforded by these complementary techniques to empirically constrain the parameters in leaky-box models of galactic chemical evolution. The emphasis is on the starburst epoch throughout, although I illustrate the impact of burst duty cycle on the time-integrated metal loss and intergalactic medium (IGM) enrichment.

1.2 Chemodynamical Modeling of Galactic Outflows

Galactic-scale outflows are driven by a large number of massive stars, so estimates of the mechanical power and metal injection rate are generally averaged over the stellar population. In this section I discuss properties of starburst synthesis models critical to galactic wind dynamics and enrichment. Metal yields from models of individual supernovae are then reviewed. Finally, I illustrate how the hydrodynamic interaction of the stellar ejecta with the ISM mixes the two fluids.

1.2.1 Energy and Metal Production by Core-collapse Supernovae

1.2.1.1 Synthesis Models

Synthesis models use a grid of stellar evolution tracks, an initial stellar mass function, and a particular star formation history to derive the effective temperature and bolometric luminosity of each star as a function of time. Observable properties are then defined by assigning a stellar atmosphere model to each star and adding all the stellar templates together. The basic trends in mass and energy production by a starburst are illustrated in Figure 1.1, which is based on the Starburst 99 synthesis models (Leitherer et al. 1999). Several properties of this mechanical feedback affect the development of galactic winds.

First, the time scales for stellar winds and supernovae differ. Stars more massive than about 20 $M_\odot$—e.g., O stars, early-B stars, and Wolf-Rayet stars—generate powerful stellar winds (Leitherer, Robert, & Drissen 1992); but all stars with masses exceeding $\sim 8\,M_\odot$ are thought to produce core-collapse supernovae (Type II) of similar energy. Following an instantaneous burst of star formation, the mass and energy deposition from supernovae will overtake the contribution from stellar winds after only a few million years. The least massive Type II supernovae explode after ~ 40 Myr.

Second, the mechanical power from supernovae is roughly constant in time. This result reflects the near-perfect cancellation between the larger number of low-mass progenitors and their longer lifetimes. The number of supernova progenitors per unit mass increases according to the Salpeter mass function, $dN \propto M^{-2.35}$, but the evolutionary rate $dM/d\tau$ slows down according to the stellar mass–lifetime relation, $\tau(M) \propto M^{-1.2}$ (Schaerer et al. 1993).

A modest burst of $10^6\,M_\odot$ generates $\sim 10^4$ supernova explosions in 40 Myr. In a starburst, these supernova are correlated spatially as well as temporally. The high pressure of the remnants drives a shock front into the surrounding interstellar gas. In a medium of uniform density, the dynamical evolution of the swept-up shell of interstellar matter is described by (Weaver et al. 1977),

$$R(t) = 104\, L_{40}^{1/5} n_0^{-1/5} t_6^{3/5} \text{ pc} \tag{1.1}$$

and

$$v(t) = 61\, L_{40}^{1/5} n_0^{-1/5} t_6^{-2/5} \text{ km s}^{-1}, \tag{1.2}$$

where the mechanical power and age are in units of 10^{40} erg s^{-1} and Myr, respectively. Since the supershell velocity is only a weak power of the starburst strength, the dynamical time scale of a galactic outflow is determined largely by the scale height of the gaseous disk, H. The time scale for a galactic wind to develop, $t_d \approx 8 \left(\frac{H}{500\text{ pc}}\right)\left(\frac{61\text{ km s}^{-1}}{v}\right)$ Myr, is longer than the lifetimes of O stars and Wolf-Rayet stars. Hence, supernovae dominate the returned energy and matter by the time a galactic outflow develops.

Finally, it should be noted that the adopted mass loss rates in synthesis models such as Starburst 99 are generally not taken directly from the stellar evolutionary models, which predict considerly higher mass loss rates than are measured. The large mass loss parameter in the stellar models probably compensates for other physical processes yet to be included

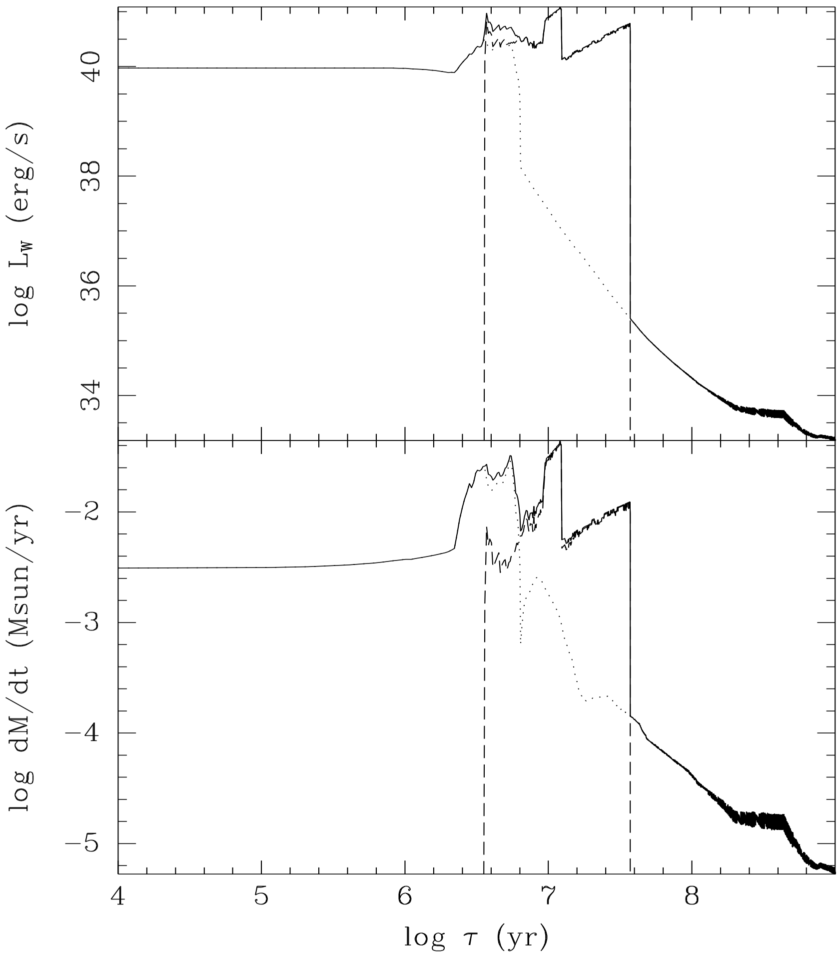

Fig. 1.1. Population synthesis models from Starburst 99 (Leitherer et al. 1999). *Top:* Production of mechanical power by a coeval starburst population. The contribution of stellar winds (dotted line) is important before a few Myr, but supernovae (dashed line) dominate at later times. *Bottom:* Mass of material returned to the ISM by stars. The curves are normalized to $10^6\ M_\odot$ of stars formed in an instantaneous burst.

in the modeling. A combination of empirical results and theoretical predictions is thought to provide a more accurate description of stellar mass loss. This prescription is sensitive to stellar metallicity in two ways (e.g., Leitherer et al. 1992). First, the ratio of Wolf-Rayet stars to O stars is metallicity dependent, and this is believed to affect the early enrichment. Second, the stellar winds grow stronger (weaker) with increasing (decreasing) metallicity because the momentum of the radiation couples to the atmosphere via metal lines. However, since the supernova properties are relatively insensitive to metallicty, neither the mass loss nor the mechanical power is sensitive to metallicity on the time scales of most galactic-scale outflows.

1.2.1.2 Supernova Yields

To determine the metal production rate, the population synthesis models must include a grid of supernova yields. I will use the models of Woosley & Weaver (1995) to illustrate some general properties. Stars in the 11–40 $M_\odot$ range produce most of the intermediate-mass elements. The 8–10 $M_\odot$ stars synthesize relatively little of these elements, so the low-mass cut-off for Type II supernovae has little impact on the ejected mass. Since increasing the minimum mass from 8 $M_\odot$ to 10 $M_\odot$ reduces the number of supernovae, the low-mass cut-off does have some affect on the mechanical feedback.

The high-mass cut-off for supernovae, in contrast to the low-mass cut-off, does affect the yield but has little impact on *the number of supernovae*. In the Woosley & Weaver (1995) models, stars heavier than 40 $M_\odot$ undergo considerable reimplosion of heavy elements, reducing their yield. The mass above which stars stop contributing to the yield is not firmly established, however. In Figure 1.2, I have weighted the Woosley & Weaver (1995) yields by a Salpeter initial mass function to illustrate the O production in various stellar mass intervals. The mass of O produced in each stellar mass interval is given per unit initial mass of 0.1–100 $M_\odot$ stars formed. The O production peaks around 30 $M_\odot$ because more massive stars retain a large fraction of their synthesized metals.

Integrating over stellar mass, the total oxygen yield is 0.0061 for the 0.1 $Z_\odot$ models and increases to 0.0065 for the solar-metallicity models. The ^{16}O isotope comprises about half of the heavy element yield from massive stars. Since ^{16}O is produced by He burning and Ne burning, its yield is not sensitive to the metallicity of the stellar model. In contrast, the yields of ^{17}O and ^{18}O scale roughly linearly with the initial metallicity of the star. (The ^{17}O is synthesized by the CNO tri-cycle during H shell burning, and α-capture on ^{14}N during He shell burning produces ^{18}O.) Since the abundance of ^{16}O is 3 to 5 orders of magnitude higher than that of ^{17}O or ^{18}O, the total mass of oxygen produced depends little on metallicity. The metallicity dependence of the O yield is illustrated in Figure 1.2. The same models give an Fe yield of 2.041×10^{-5} for the 0.1 $Z_\odot$ models.

Yield calculations vary by factors of a few among authors. The adopted ^{12}CO$(\alpha,\gamma)^{16}$O reaction rate is a critical parameter that accounts for some, but not all, of the differences. The amount of reimplosion also has an important impact on the yield through the contribution from the highest-mass stars. The models plotted use relatively low explosion energy and give a conservative O yield. The discretization into a finte number of explosion models also reduced the accuracy of the final yield of the population. The enrichment from a coeval burst takes place over a 40 Myr period, and many starbursts are observed at a slightly younger age before we can expect this enrichment to have been completed.

1.2.2 Mass Loading

The metallicity of the stellar ejecta does not provide much direct information on the chemical abundances in galactic outflows. The strong hydrodynamical interaction between the supernova fluid and the ISM generates a complex multi-phase flow that partially mixes the two fluids.

Numerical simulations have been instrumental in developing a basic understanding of the outflow dynamics (e.g., Suchkov et al. 1994; Suchkov et al. 1996; MacLow & Ferrara

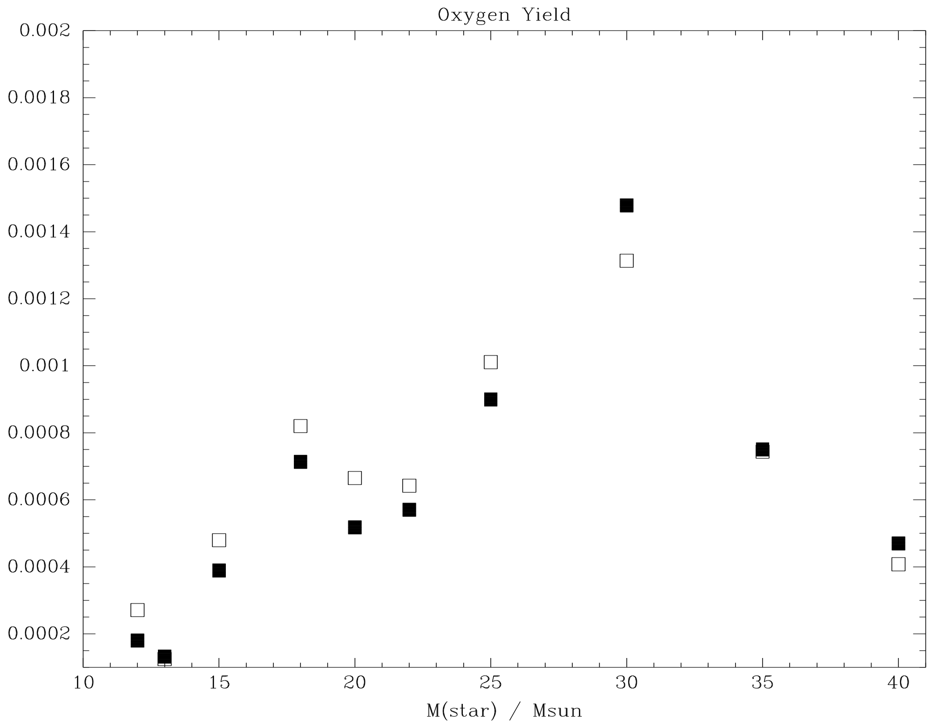

Fig. 1.2. Mass of O produced per unit mass of stars. Solid and open symbols represent 0.1 $Z_\odot$ and 1.0 $Z_\odot$ models for the initial stellar metallicity. The low explosion energy yields from Woosley & Weaver (1995) were weighted by a Salpeter initial mass function extending to 0.1 $M_\odot$. The most massive stars are rare, and they also retain a larger fraction of the synthesized oxygen. Note that stars less massive than 10 $M_\odot$ make no contribution to the total yield in this plot, so it is trivial to scale the results to other low-mass cut-offs. The total yield is 0.0061 (0.0065) per unit mass of 0.1 to 100 $M_\odot$ stars formed.

1999; Strickland & Stevens 2000). They show the collision of the wind fluid with the ISM generates shock fronts in the disk gas and the halo gas. If the outflows are fast enough, the shocked disk and halo material emits thermal X-rays. The brightness of this shocked interstellar gas can exceed that of the X-ray emission from the supernova ejecta (Suchkov et al. 1996; Strickland & Stevens 2000). The emission from the supernova fluid, usually called the *free wind*, depends on the degree of mass loading.

Mass loading takes place as the supernova ejecta punch through the galactic disk along the galaxy's minor axis. The shear at the interface between the free wind and the dense disk gas creates vortices that draw disk clouds into the free wind. The subsequent evaporation of the interstellar clouds in the hot wind fluid mixes gas with the galactic abundance pattern into the highly enriched free wind. The interstellar gas advected into these vortices is whisked into relatively dense filamentary structures. The metallicity of these cold filaments (or warm filaments if photoionized by the starburst) is that of the ambient interstellar gas. The mass of evaporated cloud material and the metallicity of the supernova ejecta determine the net metallicity of the free wind.

The X-ray observations of starburst winds empirically constrain the degree of mass loading. The X-ray emissivity increases quadratically with the gas density, so mass loading brightens outflows relative to non-loaded winds. Comparisons of data and models suggest the mass entrainment rate in M82 is 3 to 6 times larger than the mass deposition rate due to supernova (Suchkov et al. 1996). Similarly, in the dwarf starburst galaxy NGC 1569, the mass loading factor is about 9 times the mass of stellar ejecta (Martin, Kobulnicky, & Heckman 2002). *An importatnt consequence of mass loading is simply that the supernova metals are highly diluted by mixing with lower-metallicity gas.*

Figure 1.3 illustrates the dilution process for a range of supernova yields. The mass loading factor on the abscissa, χ, is defined to be the ratio of the mass of entrained ISM to the mass of supernova ejecta. Adding the entrained ISM metals to the metals from supernovae, it is straightforward to show that the wind metallicity becomes

$$Z = (Z_{\rm SN} + \chi Z_{\rm ISM})/(1+\chi), \tag{1.3}$$

where $Z_{\rm SN}$ and $Z_{\rm ISM}$ are the initial metallicities of the two fluids being mixed. The same reasoning shows the abundance ratio of α elements to iron in the wind will be,

$$Z_{\rm O}/Z_{\rm Fe} = (Z_{\rm O,SN} + \chi Z_{\rm O,ISM})/(Z_{\rm Fe,SN} + \chi Z_{\rm Fe,ISM}). \tag{1.4}$$

As more ISM is mixed into the free wind (see Fig. 1.3), the metallicity of the latter approaches that of the ambient ISM. The inflection point is determined by the ratio of initial supernova metallicity to ISM metallicity and moves to higher χ values in low-metallicity galaxies. Low-metallicity galaxies therefore present the most favorable environment for detecting supernova enrichment in galactic outflows.

1.2.3 Feedback from Type Ia Supernovae

The contribution of Type Ia supernovae to metal and energy injection is generally ignored in starburst models due to the longer evolutionary time scale of their progenitors relative to Type II supernovae. The abundance of Fe in the intracluster medium clearly indicates, however, that a significant fraction of the metals liberated by Type Ia supernovae reach the intracluster medium (Renzini 2004, and references therein). Late winds, driven by Type Ia supernova on time scales $\gtrsim 10^9$ yr, have been advocated to explain this enrichment and the mass-metallicity relation (Mathews & Baker 1972; Ciotti et al. 1991). The empirical evidence for winds, however, is mostly restricted to the early winds in starburst galaxies. The strength and ubiquity of late-type winds need to be established. Some models include Type Ia supernova progenitors as young as 100 Myr (e.g., Nomoto et al. 2003, and references therein), which, if shown to be correct, could change the way we model metal and energy feedback.

1.3 Observational Diagnostics

One of the primary challenges in describing the feedback process is understanding the mass and energy transfer between hot, warm, and cold gas in the outflows. Kinematics, composition, density, and temperatue should be measured for each component, which is not currently possible. I describe here the main techniques that are being used to measure a

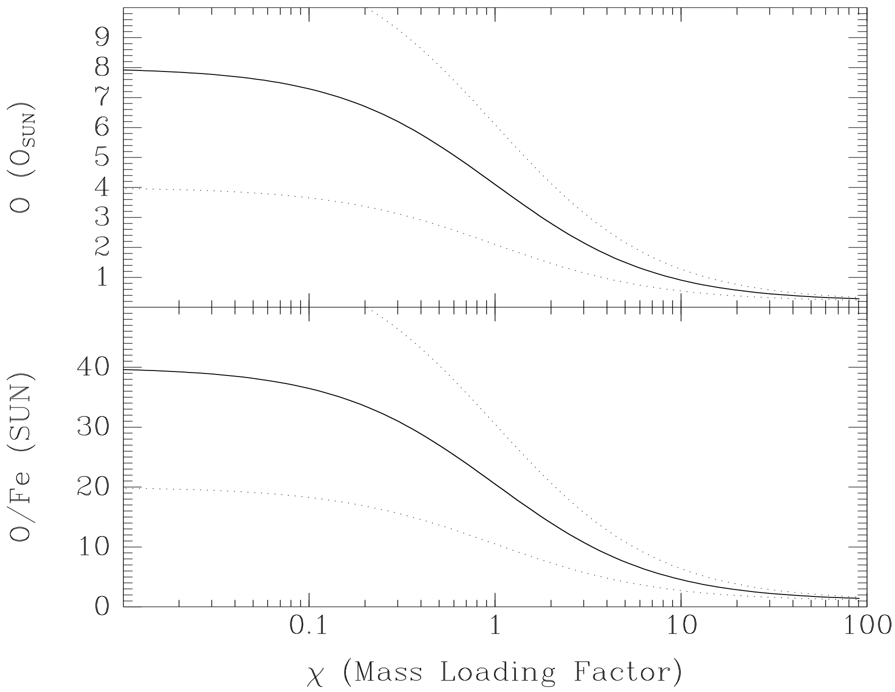

Fig. 1.3. Dilution of wind metallicity by mass entrainment. The initial mass function-averaged metallicity of supernova ejecta is ~ 8 times solar for oxygen and ~ 0.2 times solar for Fe (model A runs of Woosley & Weaver 1995 at $0.1\, Z_\odot$). The oxygen and iron yields of massive stars are only known to an accuracy of a factor of 2 to 3, so the dotted curves illustrate this range. The galactic ISM is assumed to have $0.25\, Z_\odot$ metallicity appropriate for a dwarf galaxy.

subset of these quantities. The enormous temperature range requires observations from X-ray to radio wavelengths. The data suggest the various components of the outflow undergo strong hydrodynamical and thermal interactions.

1.3.1 Optical Emission Lines

Starburst galaxies generally present moderately bright optical emission-line filaments that extend up to ~ 10 kpc out of the galactic disk (e.g., Heckman, Armus, & Miley 1990; Marlowe et al. 1995; Martin 1999). One can gain some appreciation for the excitation mechanism by considering the potential power sources. In a steady state situation, i.e. continuous star formation at a constant rate, the luminosity of the ultraviolet continuum (shortward of the ionization potential of H) is about 7 times larger than the mechanical power supplied by stellar winds and supernovae. (In a single, instantaneous burst, the ionizing luminosity only exceeds the mechanical power up to an age of 6.3 Myr when the O stars die off.) Hence, it is no surprise that the optical recombination line luminosity and the collisionally excited line luminosity are found to be dominated by emission from photoionized clouds (e.g., Lehnert & Heckman 1996; Martin 1997; Miller & Veilleux 2003).

Despite the dominance of the emission from photoionized clouds on a global scale, strong evidence for the presense of shocks is seen several kpc from the starburst region in the more extended filaments. The line ratios observed along the outflows evolve toward shock-like line ratios with increasing distance from the starburst region. Figure 2 of Martin (1997) shows several examples in dwarf starburst galaxies. Line ratios become more "shock-like" (high ratios of [N II] λ6583/Hα, [S II] λ λ6716, 6731/Hα, and [O II] λ6300/Hα) further out along the minor axis. Hybrid models that combine photoionization, shocks, and/or emission from turbulent mixing layers match the data better than photoionization alone. The rough constraints available on the chemical abundances in the dwarf starburst filaments are consistent with them being composed of disk material (Martin 1996, 1997).

The dynamics of the optical filaments were established in the seminal paper by Heckman et al. (1990). They showed that the network of Hα-emitting filaments extending along the minor axis of starburst galaxies presents double-peaked emission profiles characteristic of a moving shell. The pressure gradients indicated the shells were driven by an extended power source, and the starbursts were found to be strong enough to explain the observed shell velocities of 100–300 km s^{-1} . Subsequent studies found scaled-down versions of these flows in dwarf galaxies (Marlowe et al. 1995; Martin 1998).

For starbursts of all sizes, the estimated mass flux in the warm ionized filaments is similar to the star formation rate (SFR) (Martin 1999). This assertion rests on a volume filling factor derived from the assumption that the thermal pressure in the filaments is similar to that of the X-ray emitting region (Martin 1999). The projected velocities of the warm shells are not much larger than the escape speed, however, so much of the warm gas probably remains bound to the parent halo. The appropriate picture here may be closer to a fountain than an escaping wind. Indeed, the disks of particularly active spiral galaxies like NGC 891 and NGC 4631 also heat and transport warm gas into the halo at rates similar to the SFR per unit area.

1.3.2 X-ray Emission

The absence of local enrichment in H II regions suggests that most of the metals from core-collapse supernovae are injected directly into the hot ISM (Kobulnicky & Skillman 1996, 1997; Martin 1996). Measurements of chemical abundances from X-ray spectrocopy are therefore of great interest. In principle, abundance determinations for a collisionally ionized plasma are easier than in the nebular case in which photoionization must be included in the model. Under coronal conditions, the ionization structure is completely determined by the electron temperature, which is fixed by processes like hydrodynamic shocks.

In practice, metal abundances derived from thermal X-ray spectra are often unreliable. The observations have several biases. First, until recently, the spectral apertures were large compared to the thickness of superbubble shells. The X-ray emission within an aperture was the sum of emission from multiple components—i.e. shocked shells, mixing layers, hot bubbles, and point sources—all weighted disproportionately by the densest regions. Second, the observations were not very sensitive to gas cooler than 10^6 K or hotter than $10^{7.5}$ K. Third, due to a degeneracy between high-metallicity, two-temperature models and low-metallicity, single-temperature models, metallicities fitted to the data tended to be pushed lower than their true value if the temperature range was not fully represented (Buote & Canizares 1994). Fourth, the omission of intrinsic absorption from the spectral models increased the apparent strength of Mg and Si lines relative to Fe L lines. Unless lower-energy lines from O were detected, statistically acceptable fits could be obtained with an anomalously high α-element-to-Fe abundance ratio (e.g., Dahlem, Weaver, & Heckman 1998; Weaver, Heckman, & Dahlem 2000). Generally a volume filling factor of unity and solar abundances were simply assumed, leaving significant uncertainties about the mass and composition of the hot wind.

The *Chandra* X-ray Observatory has revolutionized our understanding of the origins of X-ray emission in starbursts. The arcsecond spatial resolution of the ACIS imaging spectrometer reveals that the brightest X-ray emitting gas lies adjacent to the warm, optical filaments. For example, in the prototypical starburst NGC 253, the X-ray emission was resolved into filaments out to 9 kpc above the disk (Strickland et al. 2000, 2002). Associations between the X-ray emission and the warm, ionized filaments have also been found in NGC 3079 (Cecil, Bland-Hawthorn, & Veilleux 2002) and in NGC 1482 and NGC 6240 (Veilleux et al. 2003). The correlation of soft X-ray emission with Hα filaments suggests the brightest X-ray emission comes from the boundary layer between the optical filaments and a hotter, undetected free wind. The extraordinary sensitivity of *XMM-Newton* has very recently detected X-ray emission over a larger region, albeit with a high degree of structure, out to 14 kpc from the disk of M82 (Stevens, Read, & Bravo-Guerrero 2003).

An ultra-deep *Chandra* exposure of perhaps the closest starburst galaxy, NGC 1569, is perhaps the best available for constraining abundances (Martin et al. 2002). The metallicity of the ISM in this galaxy is only 0.25 $Z_{\odot}$, so the contrast with supernova-enriched gas is larger than it is in more luminous starbursts. Figure 1.4 shows the ACIS spectrum of NGC 1569. At such low spectral resolution, there is no single spectral model that uniquely fits this complex spectrum. The high-resolution imaging data can break the model degeneracy, however, when combined with data obtained in optical and radio bands. For example, the X-ray color gradients reveal intrinsic absorption that is tightly correlated with the location of the 21-cm emission from the cold disk gas. The relatively hard point source component is resolved and fitted independently. The X-ray colors show there are at least two thermal emission components, and that they have different mean absorbing columns. The strong spectral lines require an α-element abundance of at least 0.25 $Z_{\odot}$ to fit the spectrum. However, the wind metallicity can be increased arbitrarily above this level provided the emission measure, which is proportional to the continuum normalization, is decreased proportionately. Using population synthesis models, normalized to the starburst in NGC 1569, to estimate the mass of supernova ejecta, which is a lower limit on the wind mass (i.e. no mass loading), the upper limit on the wind metallicity is about twice solar. The best fit implies α-element abundances in the wind of roughly solar, a mass loading factor ~ 9, and $Z_{\alpha}/Z_{Fe} \approx 3$. In NGC 1569, most of the metals in the outflow come from the supernova ejecta, not the entrained ISM, even though the ISM supplies the majority of the mass in the outflow. It appears likely that the wind carries most of the metals synthesized in the recent burst. The fraction of the total stellar mass formed in such bursts is not yet known.

1.3.3 Resonance Absorption Lines

Starburst outflows transport cold gas and dust in addition to hot gas and warm gas. When a suitably bright background light source is observed, the kinematics of the cold gas can be probed in absorption. This method probes lower column densities than the best 21-cm emission observations. The ultraviolet bandpass is preferred for absorption-line studies owing to the wide range of ionization states and elements with ultraviolet transitions. The

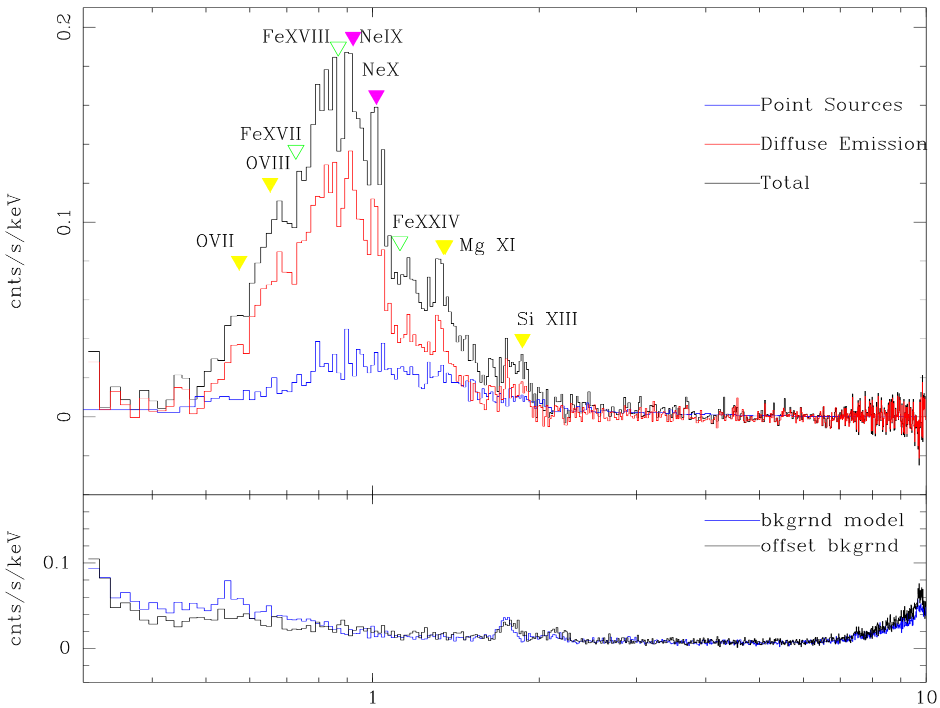

Fig. 1.4. Integrated spectrum of NGC 1569 (*top curve*). The contribution from point sources (*lower curve*) is harder than that from diffuse gas (*middle curve*). Bottom panel shows the folded X-ray background. See discussion in Martin et al. (2002), from which this figure was taken.

much higher sensitivity of ground-based telescopes means in practice that large samples of galaxies have only been observed in optical lines, particularly the Na I $\lambda\lambda$5896, 5890 doublet. Hydrogen is neutral in regions where Na I is the dominant ionization state, so the Na absorption probes the cold component of the outflow, complementing the optical emission-line and X-ray emission studies.

Most starburst galaxies show Na I absorption that is blueshifted relative to the systemic velocity (Heckman et al. 2000; Rupke, Veilleux, & Sanders 2002; Martin & Armus 2004; Schwartz & Martin 2004). The absorption is measured against star clusters in the nucleus of the host galaxy, so there is no ambiguity about the direction of the flow. Figure 1.5 summarizes the expansion velocities measured at maximum optical depth for these data sets. Taken together, there is a clear trend for the velocities to increase with increasing burst strength. The envelope is steeper than the $V \propto L_{\rm Bol}^{1/4}$ relation expected for a flow driven by a starburst of maximum surface brightness (Meurer et al. 1997; Heckman et al. 2000).

It is interesting to compare the mass flux of the cold flow to that in the warm and hot gas phases. An equivalent hydrogen column is obtained from assumptions about the Na abundance and ionization state. The inferred mass flux is particulary sensitive, however, to the size of the region the sightline represents. Heckman et al. (2000) measured an extent of

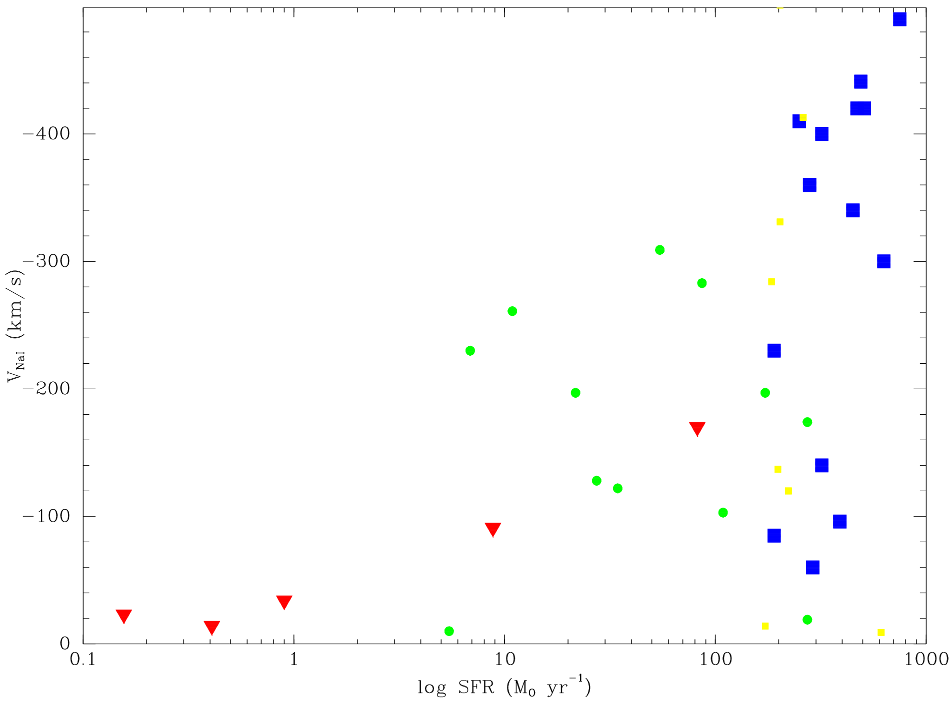

Fig. 1.5. Expansion velocity of the minimum in the Na I absorption-line profile. Filled circles represent luminous infrared galaxies from Heckman et al. (2000). Ultraluminous infrared galaxies are shown as large squares (Martin & Armus 2004) and small squares (Rupke et al. 2002). Dwarf starbursts from Schwartz & Martin (2004) are denoted by triangles. The maximum outflow velocities are larger in the more powerful starbursts.

1 to 10 kpc along their slits for the absorbing region, and they argued the cold clouds carried a mass flux similar to the SFR. Rupke et al. (2002) found the mass flux in the ultraluminous starbursts appears to be about an order of magnitude less than the SFR. Of those dwarf galaxies that show interstellar Na I absorption, the area of the outflow would need to be at least 1 kpc to bring the flux of cold material up to that of the SFR (Schwartz & Martin 2004). The neutral clouds may carry a significant fraction of the mass in the flow.

1.4 Escape to the IGM?

While hot, warm, and cold components of the outflow clearly leave the starburst region, reaching heights several kpc above the disk, the amount of mass escaping to the IGM is not yet firmly established. Here I summarize the measurements by phase. For comparison, recall that the escape velocities are at least $1.4V_c$, where V_c is the rotation speed of the disk. Simple models for an isothermal halo raise the escape velocity to 3.4 times V_c (for a halo extending 100 times further than the starburst region).

The projected expansion velocities measured in the Hα filaments reach 120 km s^{-1} in NGC 1569, whose $V_c \approx 30$ km s^{-1} , and hundreds of km s^{-1} in larger galaxies. The fraction of the warm gas mass that has been accelerated past the escape velocity cannot be measured directly due to the uncertain details of the geometry. However, most studies have concluded that the fraction of warm gas escaping is less than the total warm gas mass—often much less.

The Na I absorption studies sample the mass distribution in the wind as a function of velocity more fairly than the emission-line studies, since they measure the gas column directly and are not biased toward the densest regions. The terminal velocities in the neutral flow are much larger than the velocities of maximum optical depth shown in Figure 1.5. They reach 700 km s^{-1} in the ultraluminous starbursts (Martin & Armus 2004). These systems are mergers of L^* galaxies, however, which have rotation speeds $\sim$ 200 to 300 km s^{-1} . These terminal velocities, although large, are actually similar to the escape velocity. It is intriguing that the measured terminal velocities in the dwarf galaxies are not only lower, but once again approximately equal to the escape speed. Efforts should be made to understand why this conspiracy between the terminal velocity of the cold clouds and the escape velocity arises.

The soft X-ray emission from the wind traces a mixture of free wind and entrained material and provides the best direct detection to date of material that appears likely to escape from the galaxy and enrich the IGM. Figure 1.6 summarizes the X-ray temperatures of the diffuse emission from starburst galaxies. The temperatures exhibit no dependence on the depth of the gravitational potential. The simple interpretation is that the hot component escapes from the dwarf galaxies but is marginally bound to large galaxies (e.g., Martin 1999).

Two factors make the interpretation of Figure 1.6 more complicated. First, the emission from boundary/mixing layers is the easiest to detect; and observations are likely failing to detect the hottest component of the wind in massive starbursts (Strickland & Stevens 2000). However, upper limits on the mass carried by this hotter component indicate it does carry the bulk of the mass; it may carry significant energy (Strickland et al. 2002). Second, large gaseous halos can significantly increase the energy requirements for expelling newly processed matter (Silich & Tenorio-Tagle 2001). The dwarf irregular galaxy NGC 4449 is situated in such a halo, and the powerful outflow will probably generate little mass loss (Summers et al. 2003). The tidal interactions in the M81 group apparently affect the fate of the outflow from the compact dwarf, NGC 3077 (Ott, Martin, & Walter 2003). Yet in some dwarf galaxies like NGC 1569 (Martin et al. 2002) or Mrk 33 (Summers, Stevens, & Strickland 2001), the outflows appear destined to transport metals into the IGM.

1.5 Impact on Galactic Chemical Properties

It has been known since the early work on the stellar metallicity distribution in the solar neighborhood that the chemical evolution of the Galaxy did not proceed as a closed system. The simplicity of a closed-box model sometimes lends useful insight, however. In particular, the addition of outflows to the closed-box model, i.e. the *leaky-box* model, provides some insight into the impact of galactic winds on chemical evolution.

1.5.1 Properties of a Leaky Box

The properties of the leaky-box model were worked out by Larson (1974) and further generalized by Edmunds (1990). I will attempt to constrain the parameters of this model using the observations described in this review. Following the notation introduced by Bin-

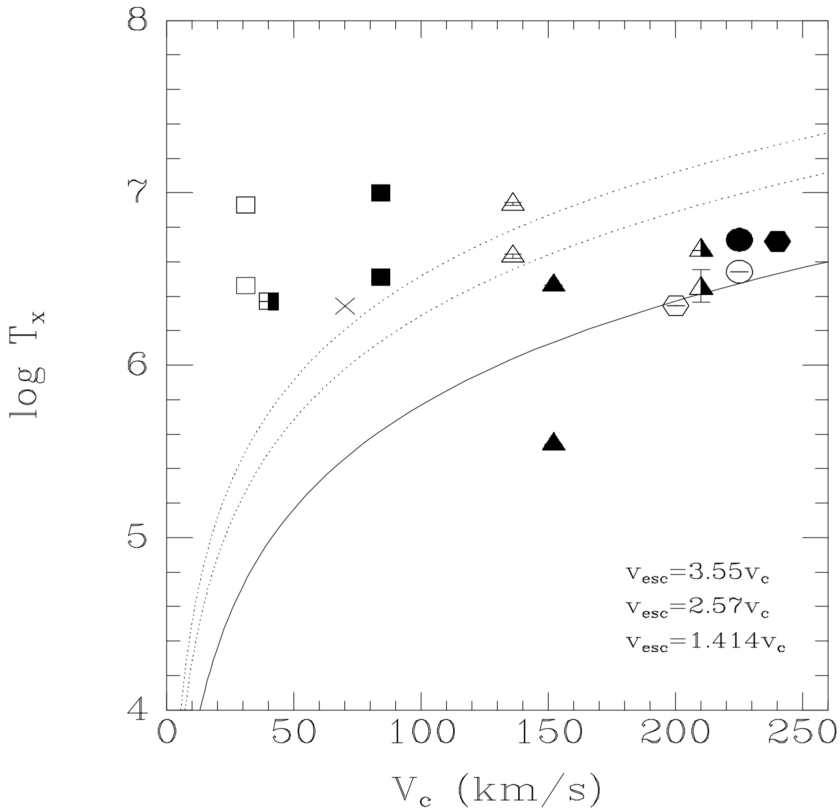

Fig. 1.6. Temperature of the diffuse X-ray emission vs. galactic rotation speed. From left to right, the galaxies are NGC 1569 (Martin et al. 2002), NGC 3077 (Ott et al. 2003), He 2-10 (Kobulnicky & Martin 2004), NGC 4449 (Summers et al. 2003), M82 (Stevens et al. 2003), NGC 4631 (Dahlem et al. 1998), NGC 3628 (Dahlem et al. 1998), NGC 253 (Strickland et al. 2002), NGC 3079 (Dahlem et al. 1998), NGC 891 (Bregman & Houck 1997), and NGC 2146 (Dahlem et al. 1998).

ney & Merrifield (1998), the key parameter is the escape efficiency—call it C—that ties the rate of mass outflow to the SFR such that

$$\frac{dM_T}{dt} = -C\frac{dM_*}{dt}. \tag{1.5}$$

It is straightforward to show, using mass conservation, that the gas-phase metallicity rises as

$$Z = \frac{-p}{1+C}\ln\left(1-(1+C)\frac{M_*}{M_T(0)}\right), \tag{1.6}$$

which is equivalent to reducing the stellar yield, p, by $(1+C)^{-1}$. Measurement of the effective yields in dwarfs are below the solar yield, consistent with the outflow scenario, but have large uncertainties due to the difficulty of measuring gas mass fraction (e.g., Garnett 2000).

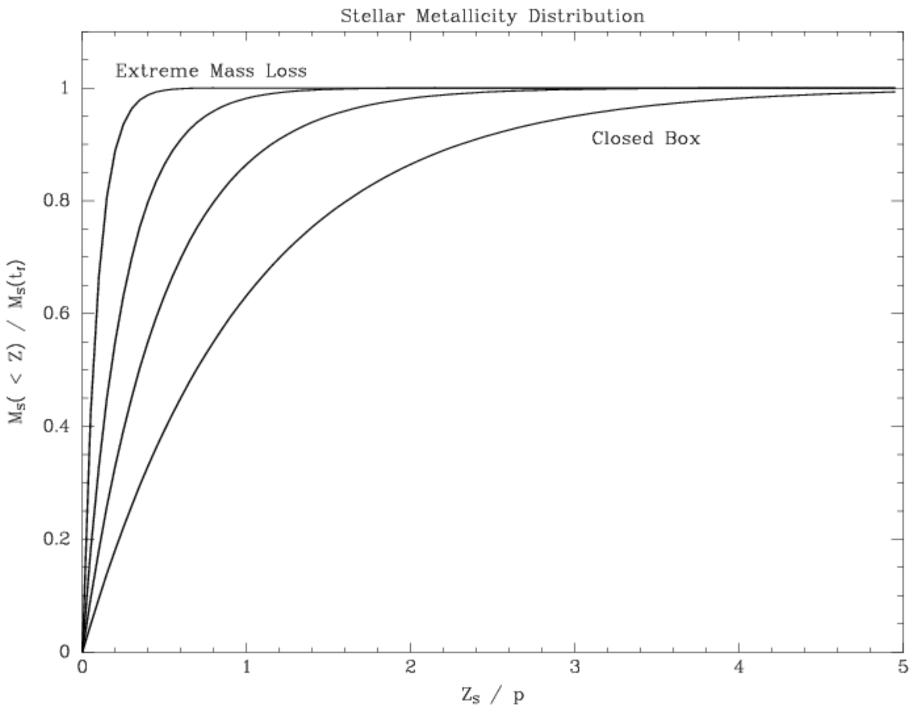

Fig. 1.7. Stellar mass distribution normalized by the total number of stars formed. Curves show values of $C = 0, 1, 3, 10$, where C is the ratio of the mass loss rate to the SFR. Note that the total mass of stars is lower in the models with mass loss.

The stellar metallicity distribution for various values of the escape efficiency is plotted in Figure 1.7. With outflow, only a fraction $(1+C)^{-1}$ of the initial mass, $M_t(0)$, is turned into stars. A larger fraction of the stars have low metallicity when strong outflows are included. In constrast, accretion of gas and the subsequent formation of additional stars from enriched gas produce a paucity of low-metallicity stars. Measurement of the stellar metallicity distribution may ultimately prove or refute the importance of outflows in dwarf galaxies.

To date, only a few stars in nearby dwarf galaxies have measured metallicities, so we can only make comparisons to the average stellar metallicity. In the leaky-box model, the average stellar metallicity reaches the effective yield, $\langle Z_* \rangle = p/(1+C)$, once gas consumption is complete. Dwarf irregular galaxies have large gas mass fractions, so the final stellar metallicity distribution is not established. The largely gas-free dwarf spheroidals, on the other hand, have reached the terminus of their chemical evolution. The measured [Fe/H] in Local Group dSphs are typically ~ -1.5, with some estimates reaching –2.0 (Mateo 1998). Outflow models would require an escape efficiency $C = 10$ to 100 to produce such low mean metallicities. Type II supernova ejecta that escapes from the galaxy cannot be incorporated into the next stellar generation of stars, so the stellar [α/Fe] ratio will be low in subsequent stellar generations. Recent measurements of the stellar [α/Fe] in dwarf spheroidals come in almost as low as the Galactic disk (Tolstoy et al. 2003), although those authors interpret the result as evidence for a truncated stellar mass function (no stars more massive than 12 $M_\odot$). In nearby starburst galaxies, the estimated outflow rates are 1 to 10 times the SFR, which is not much less than the escape efficiencies required to explain the low metallicities in the dwarf spheroidal galaxies. The higher escape efficiencies in low-mass galaxies will produce a strong correlation between mass and metallicity.

1.5.2 The Mass-metallicity Relation among Galaxies

Gas removal requires several criteria to be met. In addition to acquiring enough energy to escape from the gravitational potential, the hot gas must not radiate all of its energy or expend its energy pushing aside a massive gaseous halo.

It is easy to illustrate how the potential depth affects the escape efficiency. Let $\epsilon_{SN} = 3.75 \times 10^{15}$ erg g^{-1} be the supernova energy per unit mass of 0.1–100 $M_\odot$ stars and assume a fraction, f_{rad}, of the supernova energy is radiated away. The mass of gas that can be lifted out of the galaxy, dM_g/dt, is

$$(1 - f_{rad})\epsilon_{SN} dM_*/dt = |\phi dM_g/dt|, \tag{1.7}$$

where the gravitational potential ϕ is proportional to the square of the stellar velocity dispersion—i.e. $\phi = -f\sigma_*^2$. It follows that the escape efficiency will not exceed

$$C = \left\{ \frac{dM_g/dt}{dM_*/dt} \right\} \approx \epsilon_{SN}(1 - f_{rad})/(f\sigma_*^2). \tag{1.8}$$

The leaky-box model therefore predicts that the mean stellar metallicity grows with the potential depth as

$$\langle Z_* \rangle = \frac{p}{1+C} = \frac{p}{1 + x/\sigma_*^2}, \tag{1.9}$$

where $x \equiv \epsilon_{SN}(1 - f_{rad})/f$.

Figure 1.8 illustrates the mass-metallicity relation for various feedback parameters in the leaky-box model with $f_{rad} = 20\%$. Clearly, when σ_*^2 is small compared to ϵ_{SN}, the metallicity grows linearly with the square of the stellar velocity dispersion. Ignoring variations in mass-to-light ratio with mass, an equivalent expression is $\log \langle Z_* \rangle / p \approx 0.26 M_V + \text{constant}$, where M_V is the absolute V-band magnitude. The slope agrees very well with the relation fitted to stellar abundance measurements in dwarf spheroidals and transition objects (e.g., Mateo 1998; Fig. 7).

The agreement in slope between theory and observation has been noted previously (Larson 1974; Dekel & Silk 1986). The new aspect here is the connection to the empirical value of the feedback parameter. For example, taking the gravitational potential to be proportional to the stellar velocity dispersion and a proportionality constant $f \approx 3$, which is appropriate for an isothermal sphere, the feedback parameter C decreases from values of roughly 1000 in the smallest dwarf galaxies with σ = 10 km s^{-1} to unity in a giant galaxy with σ_* = 300 km s^{-1}. These values of C are higher than the measured range. Bringing the escape efficiency down to more reasonable values, like 0.3 and 300 in the high- and low-mass halos, respectively, requires a stronger potential with $f \approx 10$. The model with $f = 10$ in Figure 1.8 turns over very near the break at 3×10^{10} $M_\odot$ seen by Tremonti et al. (2004).

Outflows may not be a unique explanation for the strong correlation between metallicity and luminosity among dwarf galaxies. If winds are the solution, then dwarf galaxies form

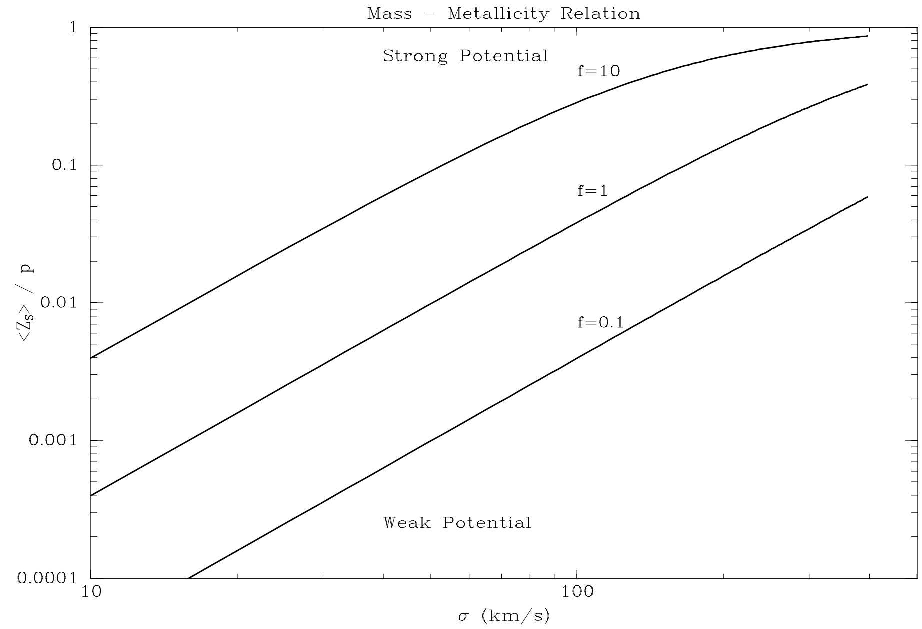

Fig. 1.8. Mass-metallicity relation for different dependences of the outflow efficiency on the potential depth. The parameter f describes the shape of the potential, such that $\phi \approx -f\sigma_*^2$.

a significant fraction of their stars in a starburst mode. The average SFR in a dSph, $\sim 10^{-4}\ M_\odot\ \mathrm{yr}^{-1}$, is not sufficient to sustain a wind from even a dwarf galaxy. However, if the duty cycle of the star formation episodes is 1% or less, then outflows become plausible. Although the dSphs clearly contain stars with a wide range of ages, it is not yet clear that the star formation histories have been resolved on a fine enough time scale to make this distinction.

1.6 Summary: Global Impact of Metal Loss via Galactic Winds

Metal ejection is now directly observed from some nearby galaxies. The importance of outflows for galaxy scaling relations and the enrichment of the IGM is still debated, however. Nearly all starburst galaxies present winds, but the fraction of stellar mass formed in starbursts is not yet known. Several factors suggest winds played a prominent role in the past.

Winds are ubiquitous in Lyman-break-selected galaxies at redshift 3–4, and these systems appear to account for at least half of the star formation at that epoch. Yet a careful census of the metals in stars and gas at redshift 2.5 recovers only 10%–15% of the metals produced by galaxies up until that time (Pettini 2003). These observations are easily reconciled if a large fraction of the metals were ejected by winds and remain in a hot, and therefore hard to detect, phase. The relatively high metallicity of the intracluster medium also suggests galaxies lose more metals than they retain (Renzini 2004).

Relic winds would be detectable in absorption long after they have faded from prominence in emission. Establishing an association with some class(es) of quasar absorption-line systems would greatly improve our understanding of the spatial extent and ubiquity of winds at high redshift. One interesting, though controversial, hypothesis is that strong Mg II systems are associated with superwinds (Bond et al. 2001). This class of absorption-line system evolves away from redshift 2 to the present, in parallel to the starburst population, and has about the right number of systems per unit redshift to be associated with starburst galaxies.

The irony of this situation is that, despite the larger escape efficiency in dwarf galaxies, the stars formed in these starburst events reside in massive galaxies today rather than in dwarf galaxies. It remains possible that winds are relatively rare in dwarf galaxies today. The star formation properties of complete samples of dwarfs selected on the basis of H I mass should resolve the role of dwarf starburst winds at the present epoch.

Acknowledgements. The author thanks Henry "Chip" Kobulnicky for discussions about the chemical evolution in galaxies. This work was supported by grants from the David and Lucile Packard Foundation and the Alfred P. Sloan Foundation.

References

Adelberger, K. L., Steidel, C. C., Shapley, A. E., & Pettini, M. 2003, ApJ, 584, 45
Binney, J., & Merrifield, M. 1998, Galactic Astronomy (Princeton: Princeton Unvi. Press)
Bond, N. A., Churchill, C. W., Charlton, J. C., & Vogt, S. S. 2001, ApJ, 562, 641
Bregman, J. N., & Houck, J. C. 1997, ApJ, 485, 159
Buote, D. A., & Canizares, C. R. 1994, ApJ, 427, 86
Cecil, G., Bland-Hawthorn, J., & Veilleux, S. 2002, ApJ, 576, 745
Ciotti, L., D'Ercole, A., Pellegrini, S., & Renzini, A. 1991, ApJ, 376, 380
Dahlem, M., Weaver, K. A., & Heckman, T. M. 1998, ApJS, 118, 401
Edmunds, M. G. 1990, MNRAS, 246, 678
Garnett, D. R. 2002, ApJ, 581, 1019
Heckman, T. M., Armus, L., & Miley, G. K. 1990, ApJS, 74, 833
Heckman, T. M., Lehnert, M. D., Strickland, D. K., & Armus, L. 2000, ApJS, 129, 493
Kobulnicky, H. A., & Martin, C. L. 2004, in preparation
Kobulnicky, H. A., & Skillman, E. D. 1996, ApJ, 471, 211
——. 1997, ApJ, 489, 636
Larson, R. B. 1974, MNRAS, 166, 585
Lehnert, M. D., & Heckman, T. M. 1996, ApJ, 462, 651
Leitherer, C., et al. 1999, ApJS, 123, 3
Leitherer, C., Robert, C., & Drissen, L. 1992, ApJ, 401, 596
MacLow, M.-M., & Ferrara, A. 1999, ApJ, 513, 142
Marlowe, A. T., Heckman, T. M., Wyse, R. F. G., & Schommer, R. 1995, ApJ, 438, 563
Martin, C. L. 1996, ApJ, 465, 680
——. 1997, ApJ, 491, 561
——. 1998, ApJ, 506, 222
——. 1999, ApJ, 513, 156
Martin, C. L., & Armus, L. 2004, in preparation
Martin, C. L., Kobulnicky, H. A., & Heckman, T. M. 2002, ApJ, 574, 663
Mateo, M. 1998, ARA&A, 36, 435
Mathews, W. G., & Baker, J. C. 1971, ApJ, 170, 241
Meurer, G., et al. 1997, AJ, 114, 54
Miller, S. T., & Veilleux, S. 2003, ApJ, 592, 79
Nomoto, K., Uenishi, T., Kobayashi, C., Umeda, H., Ohkubo, T., Hachisu, I., & Kato, M. 2003, in From Twilight to Highlight: The Physics of Supernovae, ed. W. Hillebrandt & B. Leibundgut (Berlin: Springer), 115
Ott, J., Martin, C. L., & Walter, F. 2003, ApJ, 594, 776
Pettini, M. 2003, in Cosmochemistry: The Melting Pot of Elements (Cambridge: Cambridge Univ. Press), in press (astro-ph/0303272)
Pettini, M., Rix, S. A., Steidel, C. C., Adelberger, K. L., Hunt, M. P., & Shapley, A. E. 2002, ApJ, 569, 742

Renzini, A. 2004, in Carnegie Observatories Astrophysics Series, Vol. 4: Origin and Evolution of the Elements, ed. A. McWilliam & M. Rauch (Cambridge: Cambridge Univ. Press), in press
Rupke, D. S., Veilleux, S., & Sanders, D. B. 2002, ApJ, 570, 588
Schaerer, D., Charbonnel, C., Meynet, G., Maeder, A., & Schaller, G. 1993, A&AS, 102, 339
Schwartz, C., & Martin, C. L. 2004, ApJ, submitted
Silich, S., & Tenorio-Tagle, G. 2001, ApJ, 552, 91
Stevens, I. R., Read, A. M., & Bravo-Guerrero, J. 2003, MNRAS, 343, L47
Strickland, D. K., Heckman, T. M., Weaver, K. A., & Dahlem, M. 2000, AJ, 120, 2965
Strickland, D. K., Heckman, T. M., Weaver, K. A., Hoopes, C. G., & Dahlem, M. 2002, ApJ, 568, 689
Strickland, D. K., & Stevens, I. R. 2000, MNRAS, 314, 511
Suchkov, A. A., Balsara, D. S., Heckman, T. M., & Leitherer, C. 1994, ApJ, 463, 528
Suchkov, A. A., Berman, V. G., Heckman, T. M., & Balsara, D. S. 1996, ApJ, 463, 528
Summers, L. K., Stevens, I. R., & Strickland, D. K. 2001, MNRAS, 327, 385
Summers, L. K., Stevens, I. R., Strickland, D. K., & Heckman, T. M. 2003, MNRAS, 342, 690
Tolstoy, E., Venn, K. A., Shetrone, M., Primas, F., Hill, V., Kaufer, A., & Szeifert, T. 2003, AJ, 125, 707
Tremonti, C., et al. 2004, in preparation
Veilleux, S., Shopbell, P. L., Rupke, D. S., Bland-Hawthorn, J., & Cecil, G. 2003, AJ, 126, 2185
Weaver, K. A., Heckman, T. M., & Dahlem, M. 2000, ApJ, 534, 684
Weaver, R., McCray, R., Castor, J., Shapiro, P., & Moore, R. 1977, ApJ, 218, 377
Woosley, S. E., & Weaver, T. A. 1995, ApJS, 101, 181